AD_____

Award Number: W81XWH-11-1-0232

TITLE: Feasibility of Prostate Cancer Diagnosis by Transrectal Photoacoustic Imaging

PRINCIPAL INVESTIGATOR: Hanli Liu

CONTRACTING ORGANIZATION: University of Texas at Arlington
Arlington, TX 76019

REPORT DATE: March 2012

TYPE OF REPORT: Annual

PREPARED FOR: U.S. Army Medical Research and Materiel Command
Fort Detrick, Maryland 21702-5012

REPORT DOCUMENTATION PAGE

Form Approved
OMB No. 0704-0188

1. REPORT DATE *(DD-MM-YYYY)*	2. REPORT TYPE	3. DATES COVERED *(From - To)*
01-03-2012	Annual	1 Mar 2011 - 28 Feb 2012

4. TITLE AND SUBTITLE

Feasibility of Prostate Cancer Diagnosis by Transrectal Photoacoustic Imaging

5a. CONTRACT NUMBER

5b. GRANT NUMBER
W81XWH-11-1-0232

5c. PROGRAM ELEMENT NUMBER

6. AUTHOR(S)
Hanli Liu

E-Mail: hanli@uta.edu

5d. PROJECT NUMBER

5e. TASK NUMBER

5f. WORK UNIT NUMBER

7. PERFORMING ORGANIZATION NAME(S) AND ADDRESS(ES)
University of Texas at Arlington
Arlington, TX 76019

8. PERFORMING ORGANIZATION REPORT NUMBER

9. SPONSORING / MONITORING AGENCY NAME(S) AND ADDRESS(ES)
U.S. Army Medical Research and Materiel Command
Fort Detrick, Maryland 21702-5012

10. SPONSOR/MONITOR'S ACRONYM(S)

11. SPONSOR/MONITOR'S REPORT NUMBER(S)

12. DISTRIBUTION / AVAILABILITY STATEMENT
Approved for Public Release; Distribution Unlimited

13. SUPPLEMENTARY NOTES

14. ABSTRACT

There is no effective imaging tool currently available for prostate cancer detection; needle biopsy is the current practice for diagnosis of the disease, aiming randomly in the prostate. Transrectal ultrasound has been used as a guiding tool to direct tissue needle biopsy for prostate cancer diagnosis; it cannot be utilized for detecting prostate cancer due to lack of sensitivity. Recent studies show that the combination of light and ultrasound may lead to a new imaging device that can be used to provide cancer-sensitive, ultrasound images for prostate cancer detection.

The goal of this study is to examine a new idea that combination of light and sound can lead to a better medical device so that doctors can clearly "see" harmful cancerous areas in the human prostate. The scientific basis for this idea is that when an organ is illuminated with light, cancer tissue will absorb more light and generate some heat. The light-generated heat, in turn, will be converted to sound wave and be "heard" by sound detectors. The cancerous sound waves will be plotted into images, allowing doctors "see" cancer better in the human prostate. The plan for the study includes two steps: (1) to setup the device and perform laboratory experiments using non-tissue samples, and (2) to calculate the measured data and thus to prove the new idea.

15. SUBJECT TERMS

Technology Development, optical spectroscopy, transrectal probe, optical biopsy, auto-fluorescence spectroscopy, fluorescence life-time measurement.

16. SECURITY CLASSIFICATION OF:			17. LIMITATION OF ABSTRACT	18. NUMBER OF PAGES	19a. NAME OF RESPONSIBLE PERSON
a. REPORT	b. ABSTRACT	c. THIS PAGE			USAMRMC
U	U	U	UU	14	19b. TELEPHONE NUMBER *(include area code)*

Table of Contents

2011-2012 Annual Progress Report

This report presents the specific aims and accomplishments of our prostate cancer research project during the year of funding sponsored by the US Department of the Army. It covers our activities from May 2011 to June 2012.

1. Introduction

The goal of this study is to form the hypothesis that a transrectal photo-acoustic imaging (TR-PAI) device can be developed and will significantly enhance detection of aggressive cancerous areas in the human prostate.

The project has two specific aims:

Aim 1: design and implement a laboratory-based TR-PAI system and perform laboratory experiments using tissue-blood phantoms;

Aim 2: Based on the laboratory phantom experiments, characterize the quality of reconstructed PAI, including image resolutions, position errors of the given simulated tumors, and quantification accuracy of the physiological parameters of simulated tumor tissues.

2. Body of the Report

We have carried out Aim 1 in the past 12 months; this report summarizes the work that we performed accordingly, mainly for Aim 1. We will also provide the information on the corresponding achievements obtained during this period of time, as given below.

2.1 Introduction

Optical imaging of cancer has been intensively studied in recent years due to its unique and high sensitivity to tumor endogenous (such as blood absorption) or exogenous (such as fluorophores) contrast [1,2]. When optically imaging a tumor, due to strong light scattering, optical techniques are usually limited either in penetration depth (such as a few hundred of microns for optical microscopy) or in spatial resolution (a few millimeters for optical diffuse optical tomography, DOT) [1-3]. Obviously, a tradeoff exists between the imaging depth and spatial resolution [4]. To overcome this problem, ultrasound techniques have been incorporated into optical techniques, yielding various modalities such as photoacoustic (PA) imaging [4]. It has been reported that the ratio of the imaging depth to spatial resolution can reach to ~100 for PA techniques, which is ~10 times higher than that of conventional DOT [(4)] and can be potentially used to imaging cancers in human breast, prostate, skin, thyroid, neck & head and others areas. Compared with pure ultrasound techniques, PA techniques provide optical contrast, which is usually much more sensitive to tissue functional and molecular information than ultrasound techniques, such as concentrations of tissue total hemoglobin, oxy- and deoxy-hemoglobin, and specific molecules regulating tumor growth and metastasis [4,5]. Compared with pure optical imaging methods (such as DOT), PA techniques have much higher spatial resolution and similar imaging depth [4,5]. The basic mechanism of a PA effect can be briefly explained as follows [4]: (1) tissue absorbs the energy of light illumination; (2) the absorbed energy leads to local temperature rise in the tissue; and (3) a pressure wave or sound, called the PA signal, is generated due to the thermoelastic effect when the local temperature is increased.

PA technologies have been intensively investigated recently and are considered as a valuable and potential powerful tool for both preclinical and clinical cancer imaging [4]. Currently, most PA imaging systems adopt a nanosecond pulsed laser with high pulse energy because a short light pulse can efficiently avoid energy loss due to thermal energy diffusion before the generation of PA signals, which

is the so-called thermal confinement [6]. While the mainstream of PA research community is attempting to continuously improve the performance of PA technologies and explore various applications, another direction is significantly underdeveloped, which is how to develop a simple, compact and cost-efficient PA system for the use of widespread global health, including prostate cancer detection [7]. A nanosecond pulsed laser with high pulse energy is usually extremely expensive (from tens to hundreds of thousand dollars) and bulky (usually seats on a large optical table). This may not be a problem for a large research laboratory to conduct research projects. However, in many clinical cases due to costs and spaces, it is almost impossible to conduct PA imaging when using an expensive and bulky system. In contrast, a low cost and compact PA technique may be more useful and practical for research laboratories with limited resources, office-based clinics, and global healthcare in low- or middle-income countries. To significantly reduce the cost and size of a PA imaging system, we developed a frequency-domain PA (FD-PA) system by using an inexpensive laser diode with a lock-in amplifier. This FD-PA technique is simple, compact and cost efficient but maintains decent performance compared with the expensive and bulky time-domain PA techniques. This FD-PA system is highly suitable for global health use, including prostate cancer detection.

2.2 Fundamental theories

2.2.1 Fundamental theories of frequency-domain photoacoustics [8, 9]

The wave equation of quantifying photoacoustic pressure is usually expressed as follows:

$$\left(\nabla^2 - \frac{1}{c^2}\frac{\partial^2}{\partial t^2}\right) P = \frac{-\beta}{C_P}\frac{\partial H}{\partial t} \tag{1}$$

where $P\ and\ H$ represent the photoacoustic signal and laser heating function, respectively, and c, β and C_P are the sound speed, the thermal expansion coefficient, and the heat capacity per mass of the irradiated medium at constant pressure, respectively. When the laser intensity is modulated as a sinusoidal function with a frequency of f ($\omega = 2\pi f$) and a modulated intensity amplitude of I_0, the heating function can be expressed as:

$$H = \mu_a I_0 \exp(-i\omega t) \tag{2}$$

where $\mu_a$is the absorption coefficient of the medium. When considering an infinitely long and optically thin (or small) planar or cylindrical absorber, the generated PA wave in the frequency-domain can be represented as equation (3) and (4), respectively, in which l and a are the thickness of the slab and the radius of the cylinder. When considering a small spherical absorber with a radius of a, the PA wave can be expressed as equation (5).

$$P = \frac{i\mu_a\beta I_0 cl}{2C_P}\left[\frac{sinc(\hat{q})}{sin(\hat{q})+i\hat{\rho}\hat{c}cos(\hat{q})}\right]\exp(-i\hat{q}\hat{t}), \qquad \text{(for a planer absorber)} \tag{3}$$

$$P = \frac{i\mu_a\beta I_0 ca}{C_P}\left[\frac{J_1(\hat{q})H_0^{(1)}(\hat{c}\hat{r}\hat{q})/\hat{q}}{J_1(\hat{q})H_0^{(1)}(\hat{c}\hat{q})-\hat{\rho}\hat{c}J_0(\hat{q})H_1^{(1)}(\hat{c}\hat{q})}\right]\exp(-i\hat{q}\hat{t}), \qquad \text{(for a cylindrical absorber)} \tag{4}$$

$$P = \frac{i\mu_a\beta I_0 ca}{C_P(r/a)}\left[\frac{[sin(\hat{q})-\hat{q}\cos(\hat{q})]/\hat{q}^2}{(1-\hat{\rho})(sin(\hat{q})/\hat{q})-\cos(\hat{q})+i\hat{\rho}\hat{c}sin(\hat{q})}\right]\exp(-i\hat{q}\hat{t}), \qquad \text{(for a spherical absorber)} \tag{5}$$

i is the imaginary unit ($\sqrt{-1}$) and $\hat{r}$ is the radial coordinate. J_0 and J_1 are the zeroth- and first-order Bessel functions, respectively, and $H_0^{(1)}$ and $H_1^{(1)}$ indicate zeroth- and first-order Hankel functions, respectively (the superscript in parentheses shows the kind of Hankel function). For a slab, $\hat{q} = \omega l/2c$, and $\hat{t} = \left(\frac{c}{l/2}\right)\left(t - \frac{z-l/2}{c}\right)$ are the dimensionless frequency and time, respectively. For a cylinder, $\hat{q} = \omega a/c$, and $\hat{t} = ct/a$ are the dimensionless frequency and time, respectively. For a sphere,

$\hat{q} = \omega a/c$, and $\hat{t} = \left(\frac{c}{a}\right)\left(t - \frac{r-a}{c}\right)$ are the dimensionless frequency and time, respectively. $\hat{\rho} = \rho_{in}/\rho_{out}$ and $\hat{c} = c_{in}/c_{out}$ are the dimensionless density and sound-speed parameters, respectively, where the subscripts "in" and "out" represent inside and outside the absorber, respectively.

A few indications can be found from equations (3)-(5) about the strength of the frequency-domain photoacoustic signal (P): (1) it is a sinusoidal function of time with the same frequency of ω as that of the modulated light; (2) it is proportional to the optical absorption coefficient (μ_a) of the medium in the cylinder; (3) it is proportional to the amplitude of the modulated intensity of I_0; and (4) it depends on the modulation frequency of ω via $\hat{q}$.

2.2.2 Fundamental theories of lock-in detection

A FD-PA signal is generally weaker compared with a time-domain PA signal at similar conditions (excited by a ns laser pulse) [7]. However, by using a lock-in detection technique, the signal-to-noise ratio can be significantly improved due to the extremely narrow bandwidth of the FD-PA signal (remember that FD-PA signal has the same frequency as that of the modulated light). The fundamental principle of a lock-in detection technique is briefly presented below (also see the User Manual of SR844 from Stanford Research Systems). If assuming that a sinusoidal PA signal and a sinusoidal reference signal can be expressed as follows:

$$\mathrm{V}_S = \mathrm{V}_{S0}\sin(\omega t + \theta_s) \tag{6}$$

$$\mathrm{V}_R = \mathrm{V}_{R0}\sin(\omega t + \theta_R) \tag{7}$$

where V_S and V_R represent the PA and reference signal, respectively, and V_{S0} and V_{R0} represent their amplitudes, respectively. θ_s and θ_R are their initial phases, respectively. A lock-in amplifier will multiply these two signals via a mixer and the result can be expressed as follows:

$$\begin{aligned}\mathrm{V}_{M1} &= \mathrm{V}_{S0}\mathrm{V}_{R0}\sin(\omega t + \theta_s)\sin(\omega t + \theta_R) \\ &= \tfrac{1}{2}\mathrm{V}_{S0}\mathrm{V}_{R0}\cos(\theta_R - \theta_s) + \tfrac{1}{2}\mathrm{V}_{S0}\mathrm{V}_{R0}\sin(2\omega t + \theta_R + \theta_s)\end{aligned} \tag{8}$$

The first term of the second line of the equation (8) is a DC (direct-current) signal and the second term is an AC (alternating current) signal with a frequency of 2ω. Since the AC signal can be easily filtered out by using a low pass filter, the filtered signal is reduced to:

$$\mathrm{V}_{M1+FILT} = \tfrac{1}{2}\mathrm{V}_{S0}\mathrm{V}_{R0}\cos(\theta_R - \theta_s). \tag{9}$$

It can be seen that the filtered mixed signal is dependent on the initial phase difference ($\cos(\theta_R - \theta_s)$). To extract the amplitude of the PA signal (V_{S0}), the phase of the reference signal (V_R) can be shifted by $\pi/2$, which is expressed as

$$\mathrm{V}_{R'} = \mathrm{V}_{R0}\sin(\omega t + \theta_R - \pi/2)\ . \tag{10}$$

The PA signal can be multiplied with this phase-shifted reference via the second mixer and the output signal from the second mixer can be represented as:

$$\mathrm{V}_{M2} = \tfrac{1}{2}\mathrm{V}_{S0}\mathrm{V}_{R0}\cos(\theta_R - \theta_s - \pi/2) + \tfrac{1}{2}\mathrm{V}_{S0}\mathrm{V}_{R0}\sin(2\omega t + \theta_R + \theta_s - \pi/2). \tag{11}$$

Similarly, the above signal can be filtered using a low pass filter and expressed as:

$$\mathrm{V}_{M2+FILT} = \tfrac{1}{2}\mathrm{V}_{S0}\mathrm{V}_{R0}\cos(\theta_R - \theta_s - \pi/2) = \tfrac{1}{2}\mathrm{V}_{S0}\mathrm{V}_{R0}\sin(\theta_R - \theta_s). \tag{12}$$

By combining equation (9) and (12), the amplitude of the PA signal (V_{S0}) and the initial phase difference between the PA signal and reference signal ($\Delta\theta = \theta_R - \theta_s$) can be written as:

$$V_{S0} = \frac{2}{V_{R0}}\sqrt{(V_{M1+FILT})^2 + (V_{M2+FILT})^2}, \quad (13)$$

$$\Delta\theta = \theta_R - \theta_s = tan^{-1}(V_{M2+FILT}/V_{M1+FILT}). \quad (14)$$

Since $V_{M1+FILT}$, $V_{M2+FILT}$ and V_{R0} are measurable, V_{S0} and $\Delta\theta = \theta_R - \theta_s$ can be calculated. Generally, the sensitivity of the lock-in detection is very high. It can even detect weak signals down to nano-volts. In this study, a broadband lock-in amplifier (LIA, SR844, Stanford Research Systems) will be utilized, which has two inputs (one is for PA signal and the other for the reference signal, in which a $\pi/2$ phase delay of the reference signal is internally and automatically implemented by this LIA). A function generator (FG) can provide a sinusoidal voltage signal with a frequency of ω to modulate a laser diode to generate a PA signal. A synchronized signal generated from the same FG is used as the reference signal and input to the LIA. The LIA will directly show the V_{S0} and $\Delta\theta$ on its screen as the outputs.

2.3 Measurement System and Data processing

2.3.1 Measurement system

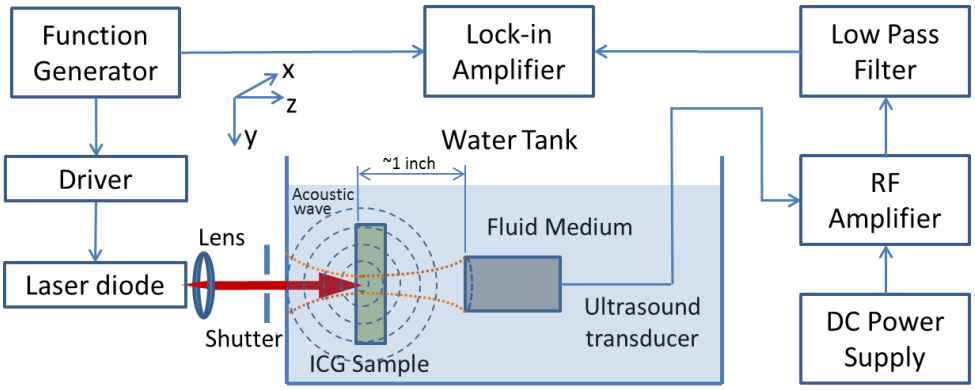

Figure 1: Experimental setup. The function generator provides sinusoidal voltage signal to the driver and further to modulate the laser diode. A synchronized TTL signal is input to the lock-in amplifier as the reference signal. The laser diode emits a modulated light beam which is focused on the sample. A shutter is used to block the laser to check background noise. The modulated light is absorbed by the sample and further emits PA waves, which is detected by the ultrasound transducer. The output voltage signal from the transducer is amplified, filtered and inputted to the lock-in amplifier. The tank is filled with a liquid medium (either water or Intralipid solution).

Figure 1 shows the experimental setup. A function generator (FG, Agilent 33120A, Agilent Tech, CA) generates a sinusoidal voltage signal and a synchronized TTL signal with the same frequency (f) and fixed phase shift. The sinusoidal signal is input into a homemade circuit to drive the laser diode (see figure 2 for details about the circuit). Thus, the laser intensity is modulated at the frequency of f. The laser diode has a central wavelength of 780 nm and a power of ~100 mW when operating in DC mode (L785P100, Thorlabs). A lens is used to collimate the laser beam and a mechanical shutter is adapted for manually blocking the laser illumination to measure the background signal. At the same time, the synchronized TTL signal from the FG is input to a lock-in amplifier (LIA, SR844, Stanford Research Systems, CA) and used as a reference signal. The sample and the ultrasound transducer (UST, Olympus NDT, one inch in focal length) are submerged into a transparent tank that is filled with either water or Intralipid solution (an optical scattering medium). The sample is indocyanine green (ICG)

aqueous solution which is injected into an optical and acoustic transparent tube (MRE-095, Braintree Scientific). The UST is focused on the sample. Both the lateral and axial sizes, (such as full width at half maximum—FWHM) of the focal zone depend on the central frequency of the UST. When the modulated laser reaches the optically absorbing sample, a PA wave is generated. The PA wave is picked up and converted into a voltage signal by the UST and further amplified (ZFL-1000LN, Mini Circuits) and filtered (SLP-5+, Mini Circuits). A total gain of 40 dB is applied by using two identical amplifiers in series that are driven by a DC power supply (BK Precision 1506). The low pass filter (SLP-5+, Mini Circuits) is not required if not available because the LIA has very narrow bandwidth. The processed PA signal is delivered to the LIA. The amplitude of the PA signal (V_{S0}) and the phase difference between the PA signal and the reference signal ($\Delta\theta$) are displayed on the screen of the LIA.

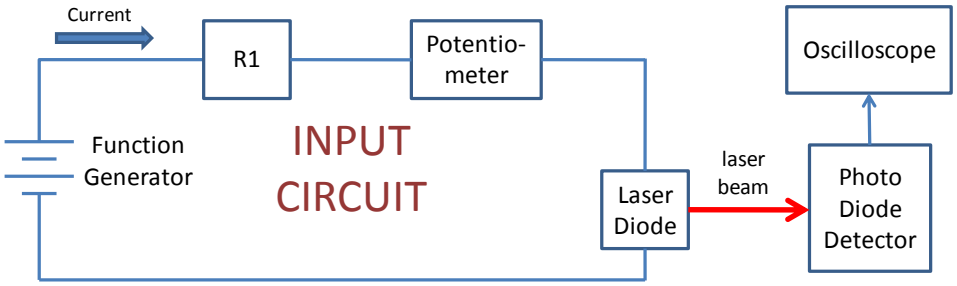

Figure 2: Principle of modulation circuit. FG provides DC and AC power to circuit. Resistor and potentiometer are chosen to provide a modulated current within the current range of the laser diode.

Figure 2 shows the principle of the modulation circuit. The principle is straightforward. The FG serves as a DC and AC power source, which means output of the FG is an AC signal with certain DC offset. A resistor (R1) and a potentiometer are used to limit and control the current flowing into the laser diode, respectively. The laser diode has a typical threshold current of 35 mA. The DC offset of the FG is V_{DC} = 2 v and the AC peak-to-peak is V_{AC} = 4 v. The total resistance of R1 and the potentiometer is ~11 ohms. A photodiode (EOT, ET-2030A) is used to verify the modulation of the laser intensity via an oscilloscope (2530B Digital Storage Oscilloscope, BK Precision)).

2.3.2 Data processing

Theoretically, the amplitude of the PA signal (V_{S0}) alone can be used to extract or represent the optical absorption coefficient (μ_a), if other parameters in equations (3)-(5) are known or can be estimated via other ways. However, in practice, it is common that the LIA shows a background signal even when the laser is turned off or blocked. This background signal is mainly caused by electronic interference from driving signal generated by the FG. Certainly, carefully shielding the system and selecting specially designed cables may be helpful to reduce this interference. However, this will require more efforts and may significantly increase the system cost. Also, it is very difficult to completely avoid this interference due to the high sensitivity of the LIA. Fortunately, this background interference is independent of the location of the UST or the sample. Therefore, a simple way to eliminate its effect is mathematically subtract it from the measured PA signal. This can be described by the following equations:

$$V_{PA}\exp(i\Delta\theta_{PA}) = V_{MR}\exp(i\Delta\theta_{MR}) - V_{BG}\exp(i\Delta\theta_{BG}) \quad (15)$$

$$V_{PA} = |V_{MR}\exp(i\Delta\theta_{MR}) - V_{BG}\exp(i\Delta\theta_{BG})| \quad (16)$$

where V_{MR} and $\Delta\theta_{MR}$ represent the LIA measured amplitude and phase when the laser is on; V_{BG} and $\Delta\theta_{BG}$ the LIA measured background amplitude and phase when the laser is blocked; and V_{PA} and $\Delta\theta_{PA}$ the wanted PA amplitude and phase. Figure 3 schematically shows the relationship among the three vectors: (1) measured signal, (2) background signal and (3) PA signal. The angle between each vector and the horizontal axis (real part) represents the phase. In this study, the V_{PA} (the amplitude of the

difference, see equation (16)) is used to represent the PA signal strength and can be used to calculate the optical absorption coefficient.

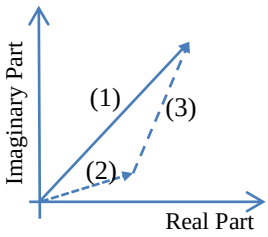

Figure 3: Measured signal is vector (1) composed of background signal (2) and PA signal (3).

2.4 Experiment, results and discussions

2.4.1. Laser modulation results

Figure 4 shows the variation of the average power of the laser diode, modulated at 1 MHz, as a function of time. Note that the laser is attenuated to avoid possible damage of the power meter (PM100D, Thorlabs), which is used to detect the laser intensity. It can be seen that there is only a 0.2% drop in intensity over 80 minutes, thus the intensity is mostly steady. Similar results were found when changing the modulation frequency from 1 MHz to 2.25 MHz or changing the modulation from a sinusoidal wave to a square wave.

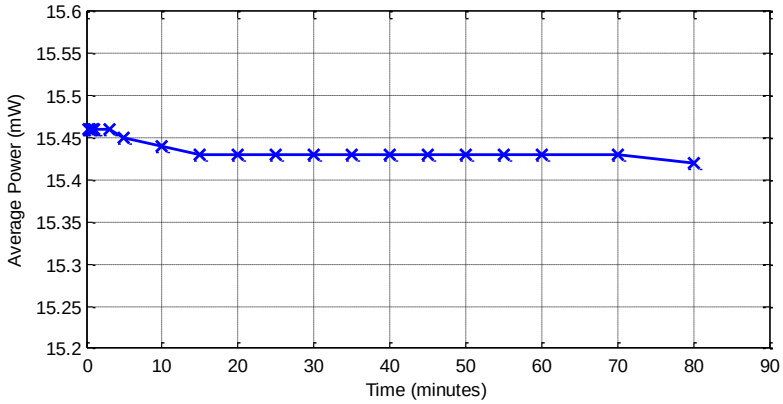

Figure 4: Measured average power of the laser diode as a function of the time. The power is stable over 80 minutes.

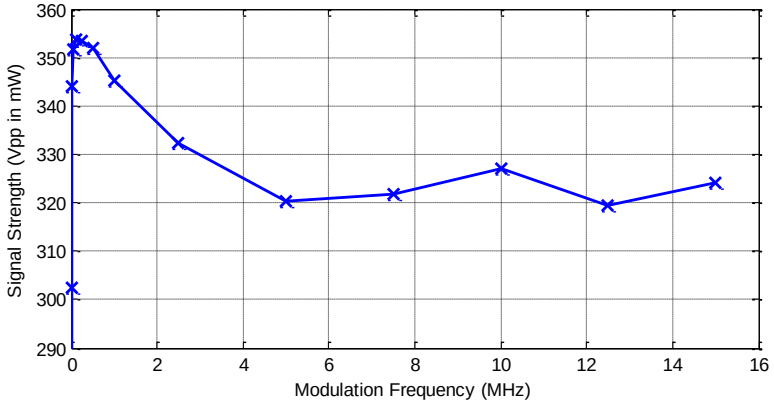

Figure 5: Laser diode signal strength as a function of the modulation frequency.

Figure 5 shows the modulation strength (peak-to-peak voltage of the AC signal, see Fig.2 for the measurement method) as a function of the modulation frequency. The frequency was varied from 1 kHz to 15 MHz. The modulation intensity decreases slightly from 50 kHz to 15 MHz. Therefore, modulating the laser diode at the UST frequencies of 1 MHz and 2.25 MHz is relatively stable.

2.4.2. Measurement of UST focal zone

To quantify the focal size of the UST, a similar technique as in Ref. [10] was adopted. Briefly, a pulser-and-receiver (5073PR Pulser/receiver, Olympus) is used to excite the UST and receive the reflected ultrasound signal. A metal wire with a small diameter (0.25 mm) is used as a sound reflector. By scanning the wire laterally and axially, the amplitude of the reflected ultrasound signal is recorded and displayed at each location. Figure 6 shows a typical result that represents a 2D ultrasound intensity distribution in the focal zone of a UST (2.25 MHz, NA=0.37). The color is proportional to the acoustic intensity. The lateral and axial FWHMs are ~0.72 mm and ~6.8 mm, respectively. Other transducers with different central frequencies have similar distribution patterns, but with different lateral and axial FWHMs. According to the principle of reciprocity, ultrasound transmission and detection of the same acoustic lens are reciprocal [11]. Therefore, the sensitivity area of detecting PA signal is considered the same as shown in figure 6.

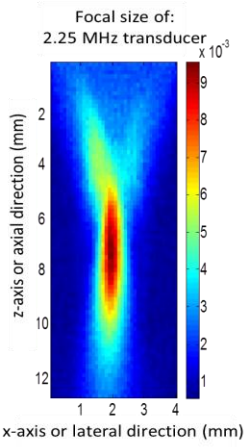

Figure 6: A 2D image showing the focal zone of the 2.25 MHz transducer. The image shows that the lateral and axial FWHMs are ~0.72 mm and ~6.8 mm, respectively.

2.4.3. Photoacoustic measurements and imaging

To simulate biological tissue, the tank was filled with 1% intralipid solution (absorption and scattering coefficients of 0.04 cm^{-1} and 8.4 cm^{-1}, respectively, measured with an ISS Oximeter). An optically and acoustically transparent tube was filled with indocyanine green (ICG) aqueous solution, at a concentration of 0.5 grams/liter, to simulate an absorbing target for generating photoacoustic signals. The tube, which has an inner and outer diameter of 1.7 mm and 2.4 mm, respectively, was positioned along the y direction.

Figure 7 shows the measured photoacoustic signal (V_{PA}) as a function of the horizontal or lateral position of the tube (along the x direction). One ultrasound transducer has a central frequency of 1 MHz and the FWHM of its lateral focal zone is about 1.3 mm. The narrow and wide rectangles represent the inner and outer diameter of the tube (1.7 mm and 2.4 mm), respectively. Clearly, the PA signals rise when the UST and laser beam gradually move into the tube region and fall when the UST and laser beam move away from the tube region. This result indicates that the highly absorbing ICG tube generates significant PA signals compared to the surrounding intralipid solution that has much lower absorption coefficient. This can be explained by equation (4) where the absorption coefficient (μ_a) is proportional to PA signal strength. The FWHM of the PA data using the 1 MHz UST in Fig. 7 is about 2.3 mm. It is larger than the tube inner diameter (1.7 mm) and the UST lateral size (1.3 mm), which can be understood that the FWHM is mainly determined by the convolution between the profile of the tube cross section and the profile of the UST lateral focal zone.

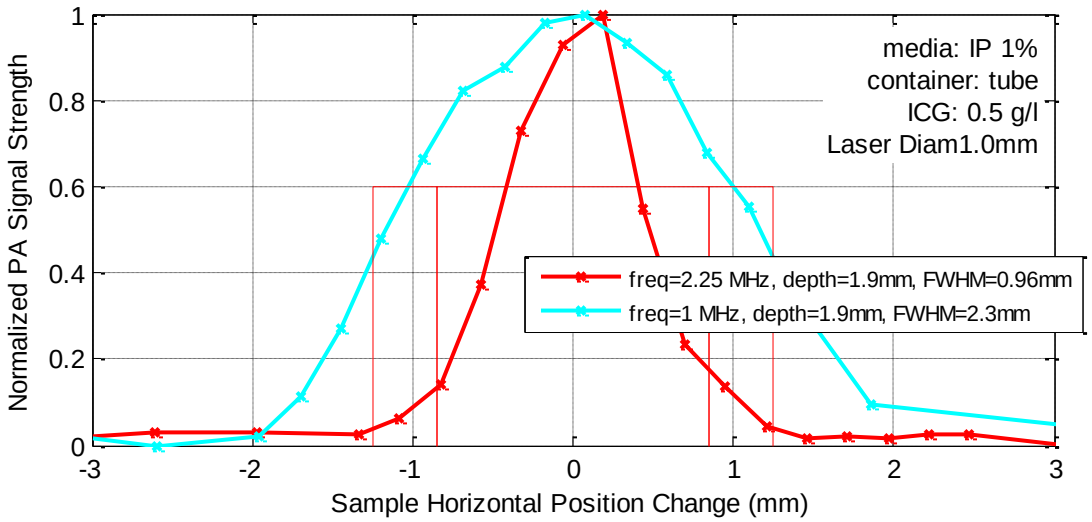

Figure 7: Normalized PA signal strength as a function of the sample horizontal location acquired from a 1 and 2.25 MHz UST. The tube is indicated by the vertical lines. UST frequency, depth of ICG, and FWHM of the PA curve are quantified in the legend.

When increasing the frequency of the UST from 1 to 2.25 MHz, the FWHM of the UST's lateral focal zone reduces from ~1.3 to ~0.72 mm. Therefore, the PA spatial resolution can be improved when using a higher frequency UST. Figure 7 illustrates this point by showing that the FWHM of the PA signal measured from the 2.25 MHz UST is 0.96 mm which is smaller than that of the PA signal measured by the 1 MHz UST (2.3 mm). However, it is also smaller than the tube size and the reason is unknown. When increasing the tube depth (from the tank wall to the surface of the tube), the PA signal strength also decreases with increasing depth as shown in Fig. 8. This is due to the light intensity I_0 (see Eq.4) which significantly reduces when depth increases because of the light scattering.

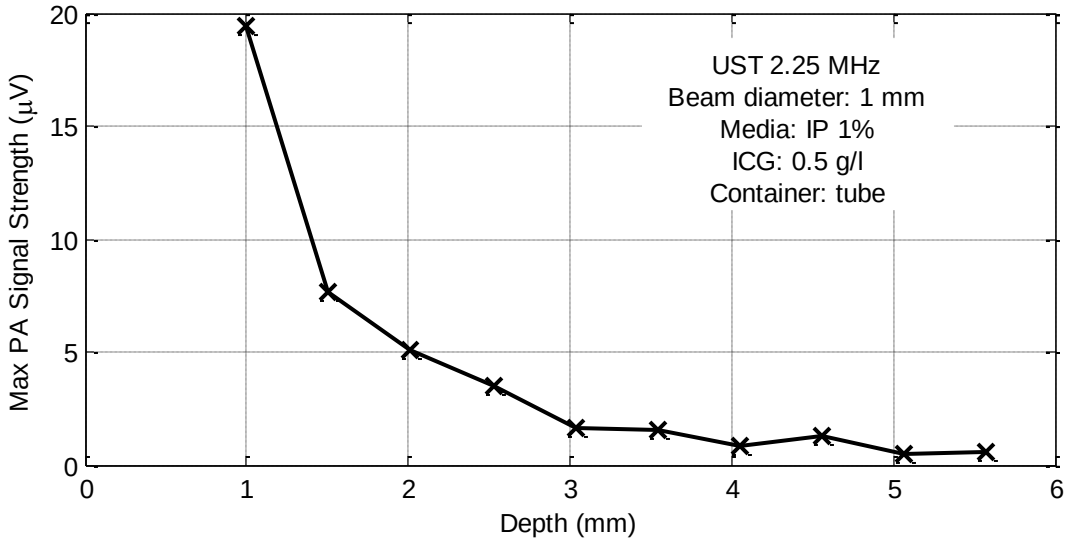

Figure 8: Maximum PA signal strength as a function of depth.

Increasing ICG concentration leads to the increase of the absorption coefficient of the tube (μ_a), which further raises the PA signal strength (see Eq.4). Figure 9 shows the peak strength of the PA signal as a function of the ICG concentration. Clearly, the PA signal increases almost linearly when the concentration is low. However, the increase of the PA signal seems saturated at high concentration.

This may be due to the fact that the light cannot penetrate into the high concentration ICG solution due to the large absorption coefficient of the high concentration ICG solution (that means that light absorption is limited at the superficial layer of the ICG solution).

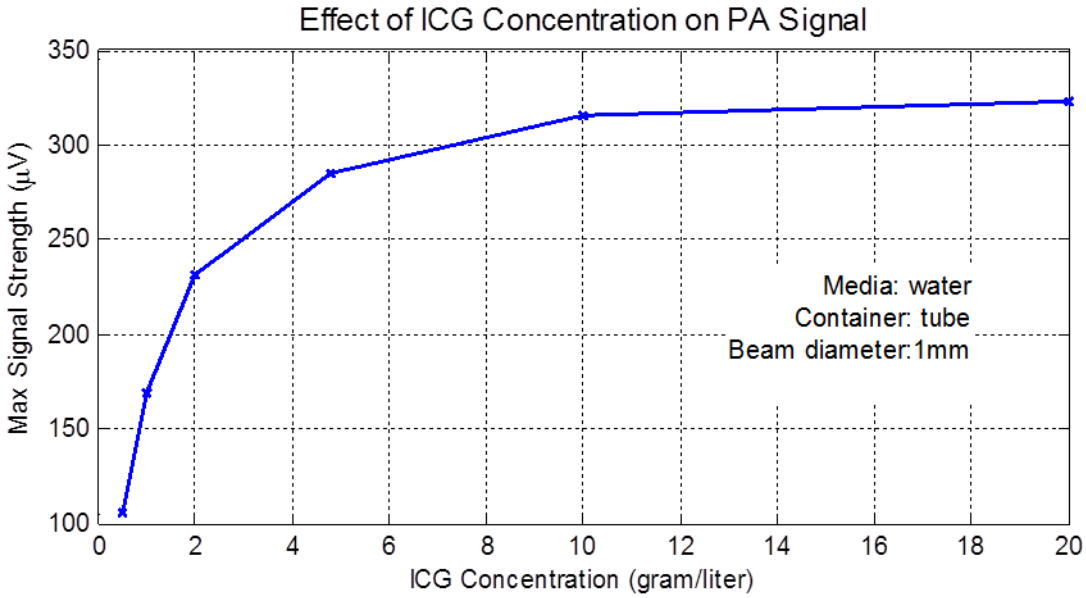

Figure 9: Effect of ICG concentration on PA signal.

Figures 10 (a) and (b) show 2-dimensional (2D) images of the tube on x-y plane (C-mode, see the coordinates in Fig.1). They were acquired from a co-registered ultrasound and PA imaging system. Briefly, the PA system is same as the one described in Fig. 1. The pure ultrasound system has the same UST as the PA system. The UST was connected with a pulse-generator-receiver (5073PR Pulser/receiver, Olympus). The reflected ultrasound data was acquired by an oscilloscope (2530B Digital Storage Oscilloscope, BK Precision). Figure 10 (c) shows the ultrasound image of the cross-section of the tube (B-mode, x-z plane). The two bright areas show the two boundaries of the tube. Note that the inner boundaries of the tube cannot be resolved from this image due to the limit resolution of the used UST (2.25 MHz). The dotted horizontal line indicates the depth of the C-mode image shown in Fig.10 (a). Clearly, the ultrasound image shows the boundaries between the tube and the surrounding medium. The FWHM is about 1.5 mm in Fig.10 (a), which is comparable with the size of the tube. Figure 10 (b) shows the corresponding PA image in the x-y plane. The image clearly shows the tube with optical (absorption) contrast. The average FWHM is about 0.88 mm, which is again smaller than the tube size (reasons are not clear).

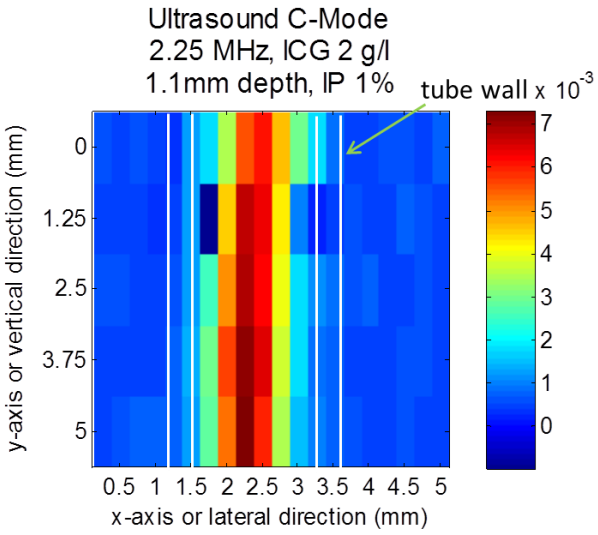

Figure 10 (a): A C-mode ultrasound image of the ICG filled tube.

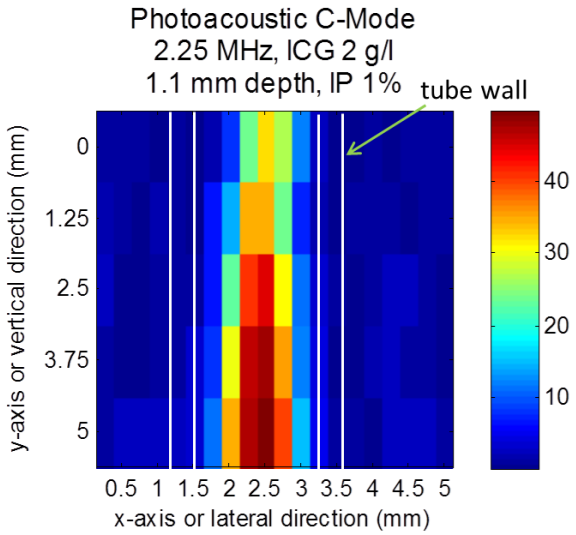

Figure 10 (b): A C-mode PA image of the same ICG filled tube.

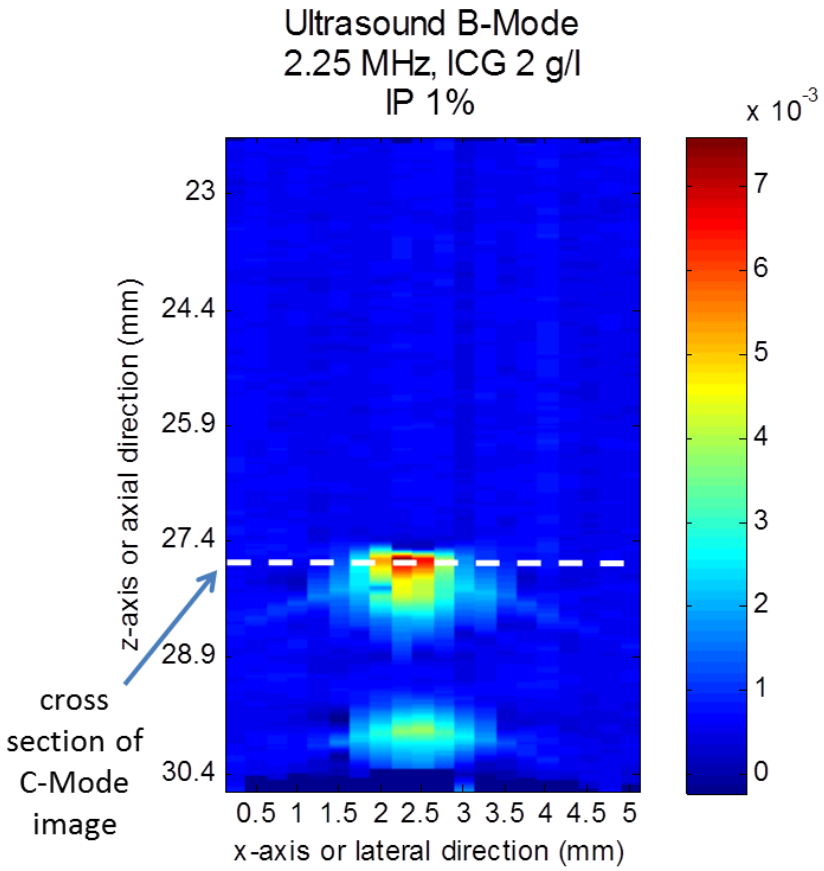

Figure 10 (c): An ultrasound B-mode image showing the cross section of the same ICG filled tube. The white dashed line indicates the depth of the C-mode image in (a).

3. Summary

We have designed, implemented, and tested a frequency-domain photoacoustic imaging system using tissue-like phantoms. The imaging principle and data processing method have been presented and verified. The measured PA signal strength depends on the absorption coefficient, depth of the target, and the modulated light intensity of the laser diode. We have learned that appropriately processing the measured PA data and background interference is an important key to correctly display the PA images. The lateral spatial resolution of PA images is dependent on ultrasound frequencies and focal size of the ultrasound transducers. Although the current system has a low axial resolution (due to the adopted ultrasound transducer), the axial resolution can be significantly improved by using a high numerical aperture ultrasound transducer or by adopting a frequency-swept technique [12]. The FD-PA imaging system is cost efficient as compared with a time-domain imaging system. Also, it is highly possible to build a compact and portable FD-PA imaging system for prostate cancer detection.

In the extended period of funding, we will further characterize the quality of reconstructed PAI, including image resolutions, position errors of the given simulated tumors, and quantification accuracy of the physiological parameters of simulated tumor tissues.

4. References

1. Corlu, A., Choe, R., Durduran, T., Rosen, M. A., Schweiger, M., Arridge, S. R., Schnall, M. D., and Yodh, A. G. (2007) Three-dimensional in vivo fluorescence diffuse optical tomography of breast cancer in humans, *Opt. Express 15*, 6696-6716.
2. Culver, J., Akers, W., and Achilefu, S. (2008) Multimodality molecular imaging with combined optical and SPECT/PET modalities, *J Nucl Med 49*, 169-172.
3. McDonald, D. M., and Choyke, P. L. (2003) Imaging of angiogenesis: from microscope to clinic, *Nature Medicine 9*, 713-725.
4. Wang, L. V. (2009) Multiscale photoacoustic microscopy and computed tomography, *Nature Photonics 3*, 503-509.
5. Wang, L. H. V. (2003) Ultrasound-mediated biophotonic imaging: A review of acousto-optical tomography and photo-acoustic tomography, *Disease Markers 19*, 123-138.
6. Xu, M., and Wang, L. (2006) Photoacoustic imaging in biomedicine, *Review of Scientific Instruments 77*, 041101.
7. Maslov, K., and Wang, L. V. (2008) Photoacoustic imaging of biological tissue with intensity-modulated continuous-wave laser, *Journal of Biomedical Optics 13*.
8. Khan, M. I., Sun, T., and Diebold, G. J. (1993) Photoacoustic waves generated by absorption of laser radiation in optically thin cylinders *Journal of the Acoustical Society of America 94*, 931-940.
9. Wang, L. (2009) In *Photoacoustic Imaging and Spectroscopy,* CRC Press.
10. Kandukuri, J., Liu, Y., and Yuan, B. (2012) A cost-efficient and multi-functional system for ultrasound measurement and imaging, *To be submitted*.
11. Wang, L., and Wu, H. (2007) Biomedical Optics: Prinicples and Imaging, John Wiley & Sons.
12. Telenkov, S., Mandelis, A., Lashkari, B., and Forcht, M. (2009) Frequency-domain photothermoacoustics: Alternative imaging modality of biological tissues, *Journal of Applied Physics 105*, 102029.